Geological characterization of a lower Cambrian marine shale: implications for shale gas potential in North-Western Hunan, South China

Xiao, Zhenghui; Liu, Jisong; Tan, Jingqiang; Yang, Rongfeng; Hilton, Jason; Zhou, Ping; Wang, Zhaohui; Cao, Yunjiang

DOI:
10.1190/INT-2017-0117.1

Document Version
Peer reviewed version

Citation for published version (Harvard):
Xiao, Z, Liu, J, Tan, J, Yang, R, Hilton, J, Zhou, P, Wang, Z & Cao, Y 2018, 'Geological characterization of a lower Cambrian marine shale: implications for shale gas potential in North-Western Hunan, South China', *Interpretation*, vol. 6, no. 3, pp. T635-T647. https://doi.org/10.1190/INT-2017-0117.1

GEOLOGICAL CHARACTERIZATION OF A LOWER CAMBRIAN MARINE SHALE: IMPLICATIONS FOR SHALE GAS POTENTIAL IN NORTH-WESTERN HUNAN, SOUTH CHINA

Zhenghui Xiao[a], Jisong Liu[a], Jingqiang Tan[b,*], Rongfeng Yang[a], Jason Hilton[c], Ping Zhou[d], Zhaohui Wang[a], Yunjiang Cao[a]

[a] Hunan Key Laboratory of Shale Gas Resource Utilization, School of Resource, Environment and Safety Engineering, Hunan University of Science and Technology, Xiangtan 411201, Hunan, China

[b] Key Laboratory of Metallogenic Prediction of Nonferrous Metals and Geological Environment Monitoring, Ministry of Education, School of Geosciences and Info-Physics, Central South University, Changsha 410083, China

[c] School of Geography, Earth and Environmental Science, University of Birmingham, Birmingham, B15 2TT, UK

[d] School of Economics, Hunan Institute of Engineering, Xiangtan 411104, Hunan, China

[*] Corresponding author: tanjingqiang@aliyun.com (J. Tan)

ABSTRACT

In this study, geological features of the lower Cambrian-aged Niutitang Shale in north-western Hunan province of South China are investigated. Results indicate that the Niutitang Shale has abundant and highly mature algal kerogen, with total organic carbon (TOC) content ranging from 0.6% to 18.2%. The equivalent vitrinite reflectance (equal-Ro) value is between 2.5% and 4.3%. Mineral constituents are dominated by quartz and clay. The average quartz content (62.8%) is much higher than that of clay minerals (26.1%) and suggests a high brittleness index. Organic-matter pores, inter-particle pores, intra-particle pores, interlaminated fractures, and structural fractures are all well developed. Porosity ranges from 0.6% to 8.8%, with an average of 4.8%, while permeability varies from 0.0018 μD (microdarcy) to 0.0600 μD (averaging 0.0182 μD). The porosity of TOC- and clay-rich shale samples is generally higher than that of quartz-rich shale samples. The gas adsorption capacity of the Niutitang Shale varies from 2.26 cm^3/g to 4.53 cm^3/g, with a mean value of 3.11 cm^3/g. The TOC content appears to significantly influence gas adsorption capacity. In general, TOC-rich samples exhibit much higher adsorption capacity than TOC-poor samples.

Keywords: lower Cambrian; Shale gas; Niutitang Shale; Unconventional oil play; Pore system; Hunan province

INTRODUCTION

The remarkable success of shale gas production in the United States has inspired substantial exploration in many other countries, particularly in China. According to a report by the United States Energy Information Administration (EIA, 2013), China holds the largest shale gas reserves globally. To secure future domestic energy supplies, the Chinese government has established plans to pursue development of shale gas and has conducted

extensive geological surveys and exploration across the country. At present, shale gas has been successfully and commercially developed from the lower Cambrian and lower Silurian shales in or near the Sichuan Basin of South China (Dang et al., 2016).

The lower Cambrian Niutitang Shale is widely distributed in north-western Hunan province, and is an important source rock for conventional petroleum in South China (Teng et al., 2006; Tan et al., 2011). More recently, this formation was also recognized as a promising unconventional shale reservoir (Tan et al., 2013).

Strategic investigations undertaken by the Ministry of Land and Resources have reported that the total shale gas reserve in north-western Hunan province is approximately 4.81×10^{12} m^3, most of which is found within the Niutitang Shale. Thus, this area has become critically important for shale gas exploration. However, scientific research performed on the Niutitang Shale is minimal when compared to shale gas prospects in the Sichuan Basin, Chongqing, and the Guizhou area (Wang et al., 2014; Zhang et al., 2015b; Tang et al., 2016).

In typical shale gas basins within North America, shale gas accumulations are generally controlled by a several factors, including the effective thickness of shale, total organic carbon (TOC) content, thermal maturity, gas content, and brittle mineral content (Curtis, 2002). The successful development of shale gas has been reported to depend on a combination of geological, geochemical, and engineering properties (Montgomery et al., 2005). The geological properties of shale plays are essential to making proper assessments of undiscovered hydrocarbon resources, to helping with the accurate application of reservoir analogues, and for the design and execution of exploration programs (Ross and Bustin, 2007; Hackley, 2012). Compared to conventional reservoirs, shales have significantly lower porosity, permeability, and matrix heterogeneity. The flow processes and related physical mechanisms in shales are thus dramatically different from those in conventional gas reservoirs (Liu et al., 2016). Successful gas extraction from shale reservoirs relies on the

application of new technologies, such as hydraulic fracturing and horizontal drilling (Li et al., 2016; Westwood, et al., 2017; Lyu, et al., 2018a and 2018b). Advances in these technologies have revolutionized shale gas production in the United States, Canada, and China.

In this study, a comprehensive geological characterization of the Niutitang Shale is provided. The TOC content, organic matter type, thermal maturity, mineral composition, physical properties of the reservoir, and gas adsorption capacity of the shale are reported. Their controls on shale gas development potential are subsequently considered. The generative processes for gas in the Niutitang Shale, and the distribution of porosity within the interval are examined. This investigation provides a comprehensive geologic framework for future shale gas exploration and production in north-western Hunan province.

GEOLOGICAL SETTING

The northwest Hunan province is located in the southeast of the Upper Yangtze Platform in South China (Fig. 1). The study area experienced a large-scale marine transgression during the latest Precambrian Ediacaran Period. To the early Cambrian, subsidence occurred, and the region developed into a shelf environment during a second transgression (Zhou et al. 2014). At this time, a ramp developed from the northwest to southeast (Wang et al., 2014). Sediments, including abundant organic matter from shallow and abyssal environments, were deposited in deep-water shelf environments (Zhou et al., 2014). The Niutitang Shale occurs at the bottom of the lower Cambrian succession, and has a total thickness ranging from 10 to 200 m (Zhang et al., 2015b). Lithologies in the lower and middle strata of the Niutitang Shale primarily consist of black shale, carbonaceous and siliceous shales that were principally formed in deep-water marine shelf and bathyal environments (Tang et al., 2016; Lin et al., 2014). Up section, the Niutitang Shale is dominated by gray to dark gray shale, silty shale,

calcareous shale, and limestone, indicative of shallow shelf environments (Tang et al., 2016; Lin et al., 2014).

MATERIALS AND METHODS

Commercial mining of the navajoite (vanadium oxide) that occurs within the black shales at the base of the Niutitang formation made fresh outcrops available for investigation in working quarries. Samples were collected form the Longshan (LS), Qiliangqiao (QLQ), Guzhe (GZ), Guzhang (GZH), Ganziping (GZP), Shancha (SC), Daping (DP), Yangjiaping (YJP), Majindong (MJD), and Shichaipo (SCP) sections (Fig. 1). Shale samples in each section were collected approximately every 10 meters through the vertical profile. A total of 82 representative samples from 10 sections were collected and analyzed in this study.

A series of measurements were performed on the selected samples, including TOC, bitumen reflectance (Rb), kerogen type, X-ray diffraction (XRD), porosity, permeability, methane adsorption isotherm, scanning electron microscopy (SEM), scanning probe microscopy (SPM), and microfocus X-ray computed tomography (μCT).

TOC content was measured using a Leco carbon−sulfur analyzer and reported as weight percentage of the rock. To analyze the sample composition and structural fabric, thin-sections were prepared for 32 samples from the lower, middle, and upper strata of each section. The types of organic matter were determined by visual inspection with a transmitted light microscope. Thermal maturity was determined according to the reflectance of solid bitumen by a MVP-3 microscope photomultiplier. A total of 26 samples were analyzed with a D/max-2600 X-ray diffractometer set to 40 kV and 30 mA to quantify the mineralogical constituents. Measured data were analyzed qualitatively using the EVA (Bruker) software, and quantitatively using the AutoQuant software. Measurements were conducted at the Research Institute of Petroleum Exploration and Development, PetroChina, Beijing.

High resolution SEM analyses, combined with the non-destructive techniques of SPM and μCT imaging, were performed on the most complete and representative samples with different TOC contents and lithofacies types. These tests were conducted at the Research Institute of Petroleum Exploration and Development, Langfang Branch, China. The SEM and SPM analyses were conducted with a TESCAN VEGA scanning probe microscope and a CSPM5500 scanning probe microscope, respectively. The μCT analyses were performed with an ACTIS-225FFI CT/DR/RTR microfocus CT scanner (BIR Corporation, USA). A detailed discussion regarding this methodology, including the measuring parameters, method, and procedures, is provided by Yao et al. (2009) and Guo et al. (2016).

Porosity and permeability were measured using an ULTRAPORE-200A Helium porosimeter and an ULTRA-PERMTM200 permeameter, respectively. These measurements were performed at room temperature (~23ºC), under normal pressure (~1.025 bar), and with 50% moisture. These analyses were also conducted at the Research Institute of Petroleum Exploration and Development, Langfang Branch, China.

Methane adsorption isotherms were generated for representative, moisture-equilibrated samples with different TOC contents under a reservoir temperature of 40 °C. The Langmuir isotherm was applied to model the gas adsorption capacity shown in equation 1.:

$$V = V_L P/(P_L + P) \quad (1)$$

Here, V is the volume of absorbed gas, V_L is the Langmuir volume (on the basis of monolayer adsorption), which is the maximum adsorption capacity of the absorbent, P is the gas pressure, and P_L is the Langmuir pressure, at which the absorbed gas content (V) is equal to half of the Langmuir volume (V_L).

RESULTS

Organic geochemistry

The TOC contents of the 82 shale samples range from 0.6% to 18.2% (Table 1), with a mean value of 5.2%, demonstrating the Niutitang Shale to have abundant organic matter. As shown in Table 2 and Figure 2, TOC varies with lithology; TOC values are high in dark, carbonaceous shales, and gradually decrease through dark shales and siliceous shales. More interestingly, thin sections and scanning probe microscopy (SPM) images reveal that the TOC content of poorly laminated shales with fine organic matter aggregates, and that of shales lacking orientation in ground matrix particles, are consistently higher than in well-laminated shales (Figs. 2 and 3).

Maceral analysis results indicate that the Niutitang Shale is principally composed of sapropel and pyrobitumen. The source materials of the organic matter were mainly algae and fungi, forming amorphous organic macerals. From this perspective, the organic matter of the Niutitang Shale is mainly an algal kerogen.

Because of the lack of vitrinite in this Early Paleozoic marine shale, the thermal maturity prediction for the Niutitang Shale is based on bitumen reflectance values. On the basis of the correlation equation (Ro=0.3195+0.6790Rb) between the bitumen reflectance (Rb) and the equivalent vitrinite reflectance (equal-Ro) established by Feng and Chen (1988) and Tan et al. (2015), the equivalent Ro values of the Niutitang Shale samples were calculated and listed in Tables 1 and 2. These equivalent %Ro values range from 2.5% to 4.3%, with a mean value of 3.2%.

Bulk mineralogy

Mineralogical data are shown in Table 2 and Fig. 4. Overall, quartz and clay are the major components, while minor constituents include feldspar, calcite, dolomite, and pyrite (Table 2). Quartz content ranges from 23.2% to 92.0% with a mean of 62.8%, while clay minerals range from 6.8% to 64.6%, with a mean of 26.1%. The total amount of brittle

minerals (i.e., quartz, feldspar, calcite, and dolomite) of the analyzed samples is higher than 70.3%, indicating that the brittleness of this shale interval is favorable for hydraulic fracturing to produce shale gas.

Physical properties

Characterization of pores and microfractures

SEM analyses, combined with non-destructive SPM and μCT imaging techniques (see Materials and Methods), were used to evaluate the pores and fractures of shale samples. Organic-matter pores, inter-particle pores (between grains), intra-particle pores (within mineral grains), interlaminated fractures, and structural fractures were all identified in the shale (Figs. 3, 5-6). Organic-matter pores (Fig. 3b) are well developed, particularly in the samples from the lower strata of the Niutitang formation, which generally have high TOC contents (mean >6%). "Honeycomb" organic-matter pores occur on the order of tens to hundreds of nanometers in diameter, and can be either elongated along the orientation of organic bands or randomly distributed (Figs. 2, 3). Inter-particle pores (Figs. 3f and l, 5a and b) occur around or between grains such as quartz, feldspars, and pyrite framboids. Intra-particle pores (Fig. 5c and d) mainly occur in clay minerals, feldspars, and pyrite framboids. Interlaminated and structural fractures (Fig. 5e and f) are both well developed in the Niutitang Shale. Interlaminated fractures occur at weak interfaces within the shale (Figs. 2f, 3e and 3h, 5e), particularly along clay flakes.

To analyze pore size, pore morphology, and the spatial distribution of pores, fractures, and minerals, three-dimensional (3D) characterization was conducted via μCT method (see Materials and Methods). The shale sample was scanned 531 times along the axial direction to obtain 531 consecutive grayscale images, which were used to produce a reconstruct 3D virtual datasets of the sample. The 3D reconstruction of the sample via the computer-aided

design (CAD) model is shown in Figure 6. The image-slices in the posterior (P) to anterior (A) direction, the top (T) to bottom (B) direction, and the right (R) to left (L) direction, respectively, are shown in Figure 6a-c. In a typical grayscale image, void spaces (e.g., pores and fractures) with low CT values appear black, and minerals with high CT values are white, while shale organic matrix with medium CT values are gray (Yao et al., 2009; Xu and Guo, 2014). As shown in Figure 6, the spatial distribution of pores, fractures, and minerals were clearly identified, and highly anisotropic in the shale sample. Set of fractures are well developed, some of which were in-filled by minerals. Pores were also well developed, most of which were organized as banded assemblages along fractures.

Porosity and permeability

Porosity and permeability results are presented in Table 3; porosity ranges from 0.6% to 8.8%, with a mean value of 4.8%, and permeability ranges from 0.0018 μD to 0.0600 μD, with an average of 0.0182 μD. These values indicate that the Niutitang Shale is characterized by low porosity and ultra-low permeability in the study area. There is no statistically significant correlation between porosity and permeability in the samples analyzed, though higher permeability is generally associated with more porous sediments (Table 3). This is indicative of a complex pore system in the shale.

Gas adsorption capacity

Methane adsorption experiments were conducted on 3 samples with different TOC and clay contents to determine the gas adsorption capacity. As shown in Figure 7, the high-pressure methane adsorption capacities (the maximum adsorbed gas amount) for the moisture-equilibrated Niutitang Shale samples varied from 2.26 cm^3/g to 4.53 cm^3/g, with a mean value of 3.11 cm^3/g.

DISCUSSION

Organic geochemistry

Organic matter type, richness, and thermal maturity generally control the amount and type of generated hydrocarbons; it follows that TOC has previously been considered to be one of the most critical parameters for shale gas self-generation, storage, and potential evaluation for industrial development (Jarvie et al., 2007; Tan, et al., 2015; Yan et al., 2016a). In addition to the current study, the TOC contents of the Niutitang Shale in northwest Hunan province have been reported to be very high, ranging from 0.2% to 23.3%, with a mean of ~5% (Wang et al., 2014; Liang et al., 2015; Tan et al., 2015; Zhang et al., 2015b; Tang et al., 2016). In Guizhou province, the average TOC contents of the lower Cambrian shale can be also as high as ~5% (Han et al., 2013; Luo et al., 2014; Zhang et al., 2015a). Meanwhile, the lower Cambrian shale in the Sichuan Basin and its marginal area has a lower TOC content of only ~3% (Nie et al., 2011; Yang et al., 2014; Yan et al., 2016b). Thus, the TOC contents of the lower Cambrian shale decrease from the Hunan and Guizhou area to the Sichuan Basin. The primary reason for this trend appears to be that the Cambrian black shale intervals in Guizhou and Hunan were deposited in deeper water shelf environments, which are more favorable for preservation of organic matter than the shallower water environments represented in Sichuan Basin. Furthermore, nutrient-rich oceanic upwelling supported large numbers of microplankton species in deep-water shelf environments that are conducive to organic matter accumulation (Hu et al., 2014; Zhang et al., 2015a). All these features suggest that TOC contents are primarily controlled by depositional sedimentary environments. Compared with the productive shales in the United States (e.g. Barnett shale; Dong et al., 2016), TOC contents in the Niutitang Shale within the study area are even higher, suggesting that the area is similarly favorable for shale gas exploration.

Kerogen typing for highly mature shales is fraught with difficulty because the original structure of kerogen has been altered by maturation. Results on the composition of organic matter within the Niutitang Shale are in agreement with previous studies demonstrating it to be dominated by algal kerogen (e.g. Wang et al., 2013; Zhou et al. 2014; Tan et al. 2015; Tang et al., 2016). Teng et al. (2006) and Tan et al. (2011) demonstrated that kerogen $\delta^{13}C$ values range from -29.1‰ to -31.7‰, with a mean value of -30.43‰, further indicating that its organic matter is dominated by algal kerogen. This is not surprising, given that land plants did not evolve until after the deposition of these lower Cambrian sediments. Moreover, it is also not surprising that the organic material in these shales is derived from marine microfossils (including phytoplankton) and macrofossils, which constitute type I kerogen (Tan et al. 2015), given their marine setting.

Generation of organic pores is thought to be related to the content of convertible organic carbon, which is controlled by the organic matter type; in particular, algal kerogen contains a high proportion of convertible organic carbon, and can generate more organic pores (Jarvie et al., 2007; Liang et al., 2014). The kerogen type of the Niutitang Shale is sapropelic (type I), which is highly favorable for organic pore formation and thus shale gas accumulation.

It has been widely documented that the Niutitang Shale has entered an over mature stage (Wang et al., 2013; Tan, et al., 2013 and 2015; Liang et al., 2015; Tang et al., 2016). Leng et al. (2014) reported that the mean Ro values for the Niutitang Shale in the study area can be as high as 3.6%, resulting from the complex and multiple periods of variable thermal alteration. The mean Ro values in the surrounding areas, such as the Sichuan Basin and Guizhou province, are also ~3% (Tan, et al., 2013 and 2015; Luo et al., 2014; Hu et al., 2014; Yan, et al., 2016a). It is worth noting that most of the reported results use the reflectance of bitumen as an indicator of thermal maturity because of the absence of vitrinite in Cambrian-

aged shales. Although the calculation method reported by Feng and Chen (1988) has been widely used to obtain an equivalent vitrinite reflectance value based on the bitumen reflectance for lower Paleozoic shales deposited in South China, the transformed data possibly deviate from the real thermal maturity level to a certain degree. Nevertheless, the organic matter in the Niutitang Shale has entered the dry gas window stage. Through Rock-Eval pyrolysis, Tan et al. (2015) found that the remaining organic matter in the shale shows extremely low remaining hydrocarbon potential, further revealing a very high thermal maturity.

During organic matter thermal evolution, a series of physical and chemical reactions occur, including the conversion of organic carbon, the decomposition of organic matter, and the generation of petroleum. Because type I organic matter is highly oil-prone and the organic matter in the Niutitang Shale is over mature and in the dry gas window stage, organic matter within the Niutitang Shale should have been exhausted, and no significant amount of further hydrocarbons should be generated. However, numerous organic pores may be formed by organic matter decomposition, and thus they could provide storage spaces for free gas, and adsorbing sites for adsorbed gas in the shale.

Mineralogy

Results from several studies demonstrate that the mineralogical compositions of the Niutitang Shale in the study area and surrounding areas are characterized by relatively high quartz content (>40%), and the total amount of brittle minerals could account for up to 60% (Tan, et al., 2014a; Yang et al., 2014; Wang et al., 2014; Luo et al., 2014; Hu et al., 2014; Yan et al., 2016a). These values indicate that most of the Niutitang Shale in the Upper Yangtze area, and especially in the study area, is of the siliceous type, suggesting that they are favorable for shale gas development.

The Carboniferous Barnett Shale natural gas reservoir in Texas, USA is mainly composed of quartz (35%-60% with an average of 45%), and less than one-third clay minerals, and the total amount of brittle minerals accounts for >60% of the total rock volume (Montgomery et al., 2005; Loucks and Ruppel, 2007; Zhang et al., 2014). These values are similar to those found in the Niutitang Shale within the study area, as noted here and in previous studies (e.g. Wang et al., 2013; Tan, et al., 2014a; Wang et al., 2014; Tang et al., 2016).

Tectonic processes and hydraulic fracturing can form large numbers of fractures at various scales within fragile strata; these processes may therefore interconnect isolated pores, and thus create migration pathways within the shale (Yang et al., 2014; Yan et al., 2016a). As mentioned previously, the minerals of the Niutitang Shale mainly consist of quartz and clay, and the total amount of brittle minerals within the analyzed samples can exceed 70%. This relatively high content of brittle minerals could facilitate hydraulic fracturing during the exploitation of shale gas.

It is well known that a higher Young's modulus and lower Poisson's ratio are conducive to greater brittleness. Tan et al. (2014a) reported that the measured Poisson's ratio of the lower Cambrian shale in the Upper Yangtze Platform is 0.25, which is lower than that of the Barnett shale (i.e., 0.27) according to Liang et al. (2014). This demonstrates that the Niutitang Shale in the study area should also respond well to fracturing during future shale gas exploitation.

Petrophysics

The inter-crystalline pores in pyrite framboids are reported to be large enough for the storage of gas molecules (Loucks et al., 2012; Wang et al., 2012). Pyrite is relatively abundant in the Niutitang Shale, and significant inter-particle pores occur between pyrite

framboids and between pyrite crystals and clay flakes (Fig. 5b). Intra-particle pores (Fig. 5d) are well developed in the clay minerals in the Niutitang Shale; this is likely due to the fact that the clay minerals are composed of illite and mixed layer I/S (Wang et al., 2014). Micropores up to tens of micrometers in diameter may develop during the illitization process (Tan et al., 2013; Wang et al., 2012; Liang et al., 2014).

The interlaminated fractures most likely originated during diagenesis. They generally occur along the lithological transition zone in horizontally laminated or banded zones, are spatially extensive, and are straight (Loucks et al., 2009). Structural fractures (Figs. 2a-c, 5f, 6) form as a result of tectonic stresses, but may also be impacted by weathering. These fractures likely resulted from orogenic events, such as the early Paleozoic Caledonian orogeny, late Triassic Indosinian orogeny, and the Cenozoic Himalayan tectonic movement.

Yang et al. (2016) have reported that the average porosity and permeability of the Niutitang Shale in the Mayang Basin of western Hunan (South China) is ~5% and 0.02 μD, respectively. Compared with the surrounding areas, such as Sichuan Basin and Guizhou province (Tan, et al., 2014a; Hu et al., 2014; Luo et al., 2014; Yang et al., 2014; Zhang et al., 2015a; Yan et al., 2016a), the Niutitang Shale in the study area exhibits relatively higher porosity, but lower permeability. Compared to the major shales in the United States, the porosity is similar to that of the Barnett Shale, which has ~4.5% porosity but nanodarcy permeability (e.g. Dong et al., 2016). Although such low permeability could significantly abate shale gas production, high brittle mineral contents in the lower Cambrian shale might be able compensate for this shortcoming by the artificial fractures induced by hydraulic fracturing.

To illustrate the relationship between rock composition and porosity, correlation analysis between contents of TOC, clay, quartz, and porosity was performed on the shale samples. Results reveal that shale samples with well-developed fractures have the highest

porosity, even if their TOC contents are very low (Table 3). SPM and SEM images of interlaminated fractures and structures are useful for confirming this conclusion (Figs. 3e and h, 5e and f). Excluding the effect of fractures in the shale, there is a strong correlation between TOC content and porosity (Fig. 8a), particularly for shale samples with high TOC contents. This suggests that the organic matter is partly responsible for porosity; this is consistent with results from other studies that show organic matter is an important contributor to micropores (e.g. Tan, et al., 2014a; Wang, et al., 2014; Bu, et al., 2015). That porosity is positively correlated with clay mineral content is also shown (Fig. 8b; $R^2 = 0.70$). SEM images of intraparticle pores in clay minerals (Fig. 5c and d) and fractures between clay mineral layers (Figs. 2f, 5e) also confirm this conclusion. This is in agreement with previous studies that indicate pores hosted by clay minerals are of sizes ranging from mesopores to macropores (Guo et al., 2016). Additionally, there is a negative correlation between porosity and quartz content (Fig. 8c), which can be attributed to diagenesis after deep burial during the geological history of the study area.

Relationship between the methane sorption capacity, TOC, and clay mineral content

The methane sorption capacity of the Niutitang Shale in northwest Hunan (3.11 cm^3/g) is slightly higher than that of the lower Cambrian shale from the Sichuan Basin (2.8 cm^3/g), or the north-western Guizhou province (3.08 cm^3/g) (Tan et al., 2014b; Zhang et al., 2015a). A strong positive correlation between methane sorption capacity and TOC content in marine shales has been suggested by many studies (Chalmers and Bustin 2008; Han et al., 2013; Gasparik et al., 2014; Wu et al, 2014). In this study, the large absorbed gas content is generally associated with the organic-rich shale (i.e., sample GZ07; see Fig. 7), indicating that the organic matter is partly responsible for adsorbing gas in this shale, a conclusion similar to those obtained by others (e.g. Wang et al., 2014; Tan et al., 2014b). The greater gas

absorption capacities of the shale samples with higher TOC contents are due to micropores associated with the organic components into which the gas can adsorb. In the study area, the Niutitang Shale has a high TOC content, ranging from 0.6% to 18.2%, with a mean value of 5.2%, suggesting high shale gas storage potential. However, for shale samples with low TOC contents (i.e., sample GZP03 and MJD04; see Fig. 7), and those with lower TOC contents and higher clay minerals (i.e., sample GZP03; see Table 2 and Fig. 7), a relatively high gas adsorption capacity was found, indicating that clay mineral content is also responsible for adsorbing gas.

CONCLUSIONS

A variety of analyses were conducted on the lower Cambrian Niutitang Shale from north-western Hunan province to evaluate its shale gas potential. TOC contents range from 0.6% to 18.2% (average 5.2%). Bitumen-derived Ro values are between 2.5% to 4.3% (mean=3.2%), indicating an over mature stage for the shale. These findings suggest that the primary generation of petroleum from organic matter is complete, and that any gas produced from the shale would be the result of secondary cracking. Quartz and clay minerals are the major mineral components of the Niutitang Shale, with a mean content of 62.8% and 26.1%, respectively. Five types of pores and fractures were identified, including organic matter pores, inter-particle pores, intra-particle pores, interlaminated fractures, and structural fractures. The porosity of the Niutitang Shale ranges from 0.6% to 8.8% (mean=4.8%), and the permeability ranges from 0.0018 μD to 0.0600 μD (mean=0.0182 μD). The shale intervals rich in organic matter and clay minerals exhibit higher porosity than the quartz-rich intervals. The gas adsorption capacity of the Niutitang Shale varies between 2.26 cm^3/g to 4.53 cm^3/g, with a mean value of 3.11 cm^3/g under the experimental conditions. Finally, it was revealed that microporous organic matter substantially contributes to gas adsorption.

ACKNOWLEDGEMENTS

This work is supported by the Open Fund of State Key Laboratory of Oil and Gas Reservoir Geology and Exploitation (PLC201302, Chengdu University of Technology), Major Project of Hunan Provincial Science and Technology Bureau (2012FJ1006), the Open Fund of Hunan Key Laboratory of Geomechanics and Engineering Safety (16GES05, Xiangtan University), and the Innovation Program (502501005, Central South University). We thank Daniel Jarvie, Hongliu Zeng, Yang Wang, and an anonymous reviewer for comments and suggestions, and Jeffrey Dick for language edits. Dr Xiao acknowledges support from the China Scholarship Council (CSC) for producing the manuscript at the University of Birmingham.

REFERENCES

Bu, H., Y. Ju, J. Tan, G. Wang, and X. Li, 2015, Fractal characteristics of pores in non-marine shales from the Huainan coalfield, eastern China: Journal of Natural Gas Science and Engineering, 24, 166-177, doi: 10.1016/j.jngse.2015.03.021.

Chalmers, G. R. L., and R. M. Bustin, 2008, Lower Cretaceous gas shales in northeastern British Columbia, Part I: Geological controls on methane sorption capacity: Bulletin of Canadian Petroleum Geology, 56, 1–21, doi: 10.2113/gscpgbull.56.1.1.

Curtis, J. B., 2002, Fractured shale-gas systems: AAPG Bulletin, 86, 1921-1938, doi: 10.1306/61EEDDBE-173E-11D7-8645000102C1865D.

Dang, W., J. Zhang, X. Tang, Q. Chen, S. Han, Z. Li, X. Du, X. Wei, M. Zhang, J. Liu, J. Peng, and Z. Huang, 2016, Shale gas potential of Lower Permian marine-continental transitional black shales in the Southern North China Basin, central China: Characterization

of organic geochemistry. Journal of Natural Gas Science & Engineering, 28, 639–650, doi: 10.1016/j.jngse.2015.12.035.

Dong, D., Y. Wang, X. Huang, C. Zhang, Q. Guan, J. Huang, S. Wang, and X. Li, 2016, Discussion about geological characteristics, resource evaluation methods and its key parameters of shale gas in China: Natural Gas Geoscience, 27, 1583–1601, doi: 10.11764/j.issn.1672-1926.2016.09.1583.

Feng, G., and S. Chen, 1988, Relationship between the reflectance of bitumen and vitrinite in rock: Natural Gas Industry, 8, 20-25.

Gasparik, M., P. Bertier, Y. Gensterblum, A. Ghanizadeh, B. M. Krooss, and R. Littke, 2014, Geological controls on the methane storage capacity in organic-rich shales: International Journal of Coal Geology, 123, 34–51, doi: 10.1016/j.coal.2013.06.010.

Guo, X., S. He, S. Chen, X. Chen, S. Wang, and L. Qin, 2016, Research on microstructure of shale pores and distribution features based on nano-CT scanning and digital core analysis: Coal Geology of China, 28, 28–34.

Hackley, P.C., 2012. Geological and geochemical characterization of the Lower Cretaceous Pearsall Formation, Maverick Basin, south Texas: A future shale gas resource? AAPG Bulletin, 96, 1449–1482, doi: 10.1306/11221111071.

Han, S., J. Zhang, Y. Li, B. Horsfield, X. Tang, W. Jiang, and Q. Chen, 2013, Evaluation of lower Cambrian shale in Northern Guizhou Province, South China: implications for shale gas potential: Energy & Fuels, 27, 2933–2941, doi: 10.1021/ef400141m.

Hu, M., Q. Deng, and Z. Hu, 2014, Shale gas accumulation conditions of the Lower Cambrian Niutitang Formation in Upper Yangtze region: Oil & Gas Geology, 35, 272–279, doi: 10.11743/ogg20140215.

Jarvie, D. M., R. J. Hill, and T. E. Ruble, 2007, Unconventional shale-gas systems: The Mississippian Barnett Shale of north-central Texas as one model for thermogenic shale-gas assessment: AAPG Bulletin, 91, 475–499, doi: 10.1306/12190606068.

Leng, J., J. Han, F. Li, P. Li, and L. Meng, 2014, Exploration potential of shale gas in Huayuan block, northwest Hunan province: Natural Gas Geoscience, 25, 624–631, doi: 10.11764/j.issn.1672-1926.2014.04.0624.

Liang, C., Z. Jiang, C. Zhang, L. Guo, Y. Yang, and J. Li, 2014, The shale characteristics and shale gas exploration prospects of the Lower Silurian Longmaxi shale, Sichuan Basin, South China: Journal of Natural Gas Science & Engineering ,21, 636–648, doi: 10.1016/j.jngse.2014.09.034.

Liang, F., Y. Zhu, C. Ma, H. Zhou, H. Wang, W. Bai, Q. Zhang, and H. Cui, 2015, Sedimentary distribution and reservoir characteristics of shale gas reservoir of Niutitang Formation in Northwestern Hunan: Journal of China Coal Society, 40, 2884–2892, doi: 10.13225/j.cnki.jccs.2015.0289.

Lin, T., J. Zhang, B. Li, S. Yang, W. He, X. Tang, L. Ma, and S. Pei, 2014, Shale gas accumulation conditions and gas-bearing properties of the Lower Cambrian Niutitang Formation in Well Changye 1, northwestern Hunan: Acta Petrolei Sinica, 35, 839–846, doi: 10.7623/syxb201405003.

Loucks, R. G., and S. C. Ruppel, 2007, Mississippian Barnett Shale: Litho-facies and depositional setting of a deep -water shale-gas succession in the Fort Worth Basin, Texas: AAPG Bulletin, 91, 579–601, doi: 10.1306/11020606059.

Loucks, R. G., R. M. Reed, S. C. Ruppel, and U. Hammes, 2012, Spectrum of pore types and networks in mudrocks and a descriptive classification for matrix-related mudrock pores: AAPG Bulletin, 96, 1071–1098, doi: 10.1306/08171111061.

Loucks, R. G., R. M. Reed, S. C. Ruppel, and D. M. Jarvie, 2009, Morphology, genesis, and distribution of nanometer-scale pores in siliceous mudstones of the Mississippian Barnett shale: Journal of Sedimentary Research, 79, 848–861, doi: 10.2110/jsr.2009.092.

Luo, C., S. Liu, W. Sun, B. Ran, Z. Yong, D. Yang, X. Zhang, S. Wang, Y. Ye, and B. Deng, 2014. Basic characteristics of shale gas in the Lower Cambrian Niutitang Formation in the Upper Yangtze region: taking Nangao section in Danzhai as an example: Natural Gas Geoscience, 25, 453–470, doi: 10.11764/j.issn.1672-1926.2014.03.0453

Lyu, Q., X. Long, P. G. Ranjith, J. Tan, and Y. Kang, 2018, Experimental investigation on the mechanical behaviours of a low-clay shale under water-based fluids: Engineering Geology, 233, 124–138, doi: 10.1016/j.enggeo.2017.12.002.

Lyu, Q., X. Long, P. G. Ranjith, J. Tan, Y. Kang, and Z. Wang, 2018, Experimental investigation on the mechanical properties of a low-clay shale with different adsorption times in sub-/super-critical CO_2: Energy, 147, 1288–1298, doi: 10.1016/j.energy.2018.01.084.

Montgomery, S. L., D. M. Jarvie, K. A. Bowker, and R. M. Pallastro, 2005, Mississippian Barnett shale, Fort Worth basin, north-central Texas: Gas-shale play with multi-trillion cubic foot potential: AAPG Bulletin, 89, 155–175, doi: 10.1306/09170404042.

Nie, H., J. Zhang, and Y. Li, 2011, Accumulation conditions of the Lower Cambrian shale gas in the Sichuan Basin and its periphery: Acta Petrolei Sinica, 32, 959–967.

Ross, D. J. K., and R. M. Bustin, 2007, Shale gas potential of the Lower Jurassic Gordondale Member, northeastern British Columbia, Canada: Bulletin of Canadian Petroleum Geology, 55, 51–175, doi: 10.2113/gscpgbull.55.1.51.

Slatt, R. M., and N. R. O'Brien, 2011, Pore types in the Barnett and Woodford gas shales: Contribution to understanding gas storage and migration pathways in fine-grained rocks: AAPG Bulletin, 95, 2017–2030, doi: 10.1306/03301110145.

Tan, J., B. Horsfield, R. Fink, B. Krooss, H. Schulz, E. Rybacki, J. Zhang, C. J. Boreham, G. vn Graas, and B. A. Tocher, 2014, Shale gas potential of the major marine shale formations in the Upper Yangtze platform, South China, Part III: mineralogical, lithofacial, petrophysical, and rock mechanical properties: Energy & Fuels, 28, 2322–2342, doi: 10.1016/j.fuel.2014.03.064.

Tan, J., B. Horsfield, N. Mahlstedt, J. Zhang, R. di Primio, T. A. T. Vu, C. J. Boreham, G. van Graas, and B. A. Tocher, 2013, Physical properties of petroleum formed during maturation of Lower Cambrian shale in the upper Yangtze Platform, South China, as inferred from PhaseKinetics modeling: Marine & Petroleum Geology, 48, 47–56, doi:10.1016/j.marpetgeo.2013.07.013.

Tan, J., B. Horsfield, N. Mahlstedt, J. Zhang, C. J. Boreham, D. Hippler, G.van Grass, and B. A. Tocher, 2015, Natural gas potential of Neoproterozoic and lower Palaeozoic marine shales in the Upper Yangtze Platform, South China: geological and organic geochemical characterization: International Geology Review, 57, 305–326, doi: 10.1080/00206814.2015.1004200.

Tan, J., P. Weniger, B. Krooss, A. Merkel, B. Horsfield, J. Zhang, C. J. Boreham, G. van Graas, and B. A. Tocher, 2014, Shale gas potential of the major marine shale formations in the Upper Yangtze Platform, South China, Part II: Methane sorption capacity: Fuel, 129, 204–218, doi: 10.1016/j.fuel.2014.03.064.

Tan, J., W. Wang, Y. Wang, Y. Wu, X. Wu, W. Zhao, J. Wang, and M. Zhao, 2011, Marine source rock assessment for Lower Cambrian Niutitang Formation in middle and upper Yangtze region: Marine Geology Frontiers, 27, 23–27.

Tang, S., E. Fan, S. Zhang, and W. Jiang, 2016, Reservoir characteristics and gas-bearing capacity of the Lower Palaeozoic marine shales in Northwestern Hunan: Earth Science Frontiers, 23, 135–146, doi: 10.13745/j.esf.2016.02.014.

Tenger, C., L. Gao, K. Hu, W. Pan, C. Zhang, C. Fang, and Q. Cao, 2006, High quality source rocks in the lower combination in southeast Upper Yangtze area and their hydrocarbon generation potential: Petroleum Geology & Experiment, 28, 254–259.

Wang, Y., Y. Zhu, S. Chen, and W. Li, 2014, Characteristics of the nanoscale pore structure in Northwestern Hunan shale gas reservoirs using field emission scanning electron microscopy, high-pressure mercury intrusion, and gas adsorption: Energy Fuels, 28, 945–955, doi: 10.1021/ef402159e.

Wang, Y., Y. Zhu, S. Chen, X. Zhang, and J. Zhang, 2013, Formation conditions of shale gas in Lower Cambrian Niutitang formation, northwestern Hunan: Journal of China University of Mining & Technology, 42, 586–594.

Wang, Y., D. Dong, J. Li, S. Wang, X. Li, L. Wang, K. Cheng, and J. Huang, 2012, Reservoir characteristics of shale gas in Longmaxi Formation of the Lower Silurian, Southern Sichuan: Acta Petrolei Sinica, 33, 551–561.

Wu, Y., T. Fan, J. Zhang, S. Jiang, Y. Li, J. Zhang, and C. Xie, 2014, Characterization of the upper Ordovician and lower Silurian marine shale in northwestern Guizhou province of the upper Yangtze block, South China: Implication for shale gas potential: Energy & Fuels, 28, 3679–3687, doi: 10.1021/ef5004254.

Xu, Z., and S. Guo, 2014, Application of NMR and X-CT technology in the pore structure study of shale gas reservoirs: Advances in Earth Science, 29, 624–631, doi: 10.11867/j.issn.1001-8166.2014.05.0624.

Yan, J., Y. Men, Y. Sun, Q. Yu, W. Liu, H. Zhang, J. Liu, J. Kang, S. Zhang, H. Bai, and X. Zheng, 2016, Geochemical and geological characteristics of the Lower Cambrian shales in the middle-upper Yangtze area of South China and their implication for the shale gas exploration: Marine & Petroleum Geology, 70, 1–13, doi: 10.1016/j.marpetgeo.2015.11.010.

Yan, J., Q. Li, and X. Zhu, 2016, Main factors controlling shale gas accumulation and exploration targets in the Lower Cambrian Sichuan Basin and its periphery: Petroleum Geology & Experiment, 38, 445–452, doi: 10.11781/sysydz201604445.

Yang, F., Z. Ning, and H. Liu, 2014, Fractal characteristics of shales from a shale gas reservoir in the Sichuan Basin, China: Fuel, 115, 387–384, doi: 10.1016/j.fuel.2013.07.040.

Yang, X., T. Fan, and Y. Wu, 2016, Lithofacies and cyclicity of the Lower Cambrian Niutitang Shale in the Mayang Basin of western Hunan, South China: Journal of Natural Gas Science & Engineering, 28, 74–86, doi: 10.1016/j.jngse.2015.11.007.

Yao, Y., D. Liu, Y. Che, D. Tang, S. Tang, and W. Huang, 2009, Non-destructive characterization of coal samples from China using microfocus X-ray computed tomography: International Journal of Coal Geology, 80, 113–123, doi: 10.1016/j.coal.2009.08.001.

Zhang, J., T. Fan, J. Li, J. Zhang, Y. Li, Y. Wu, and W. Xiong, 2015, Characterization of the Lower Cambrian shale in the northwestern Guizhou province, South China: implications for shale-gas potential: Energy & Fuels, 29, 6383–6393, doi: 10.1021/acs.energyfuels.5b01732.

Zhang, L., J. Guo, P. Jiao, C. Shu, and J. Li, 2015, Geological conditions and favourable exploration zones of shale gas in Niutitang Formation at northwest Hunan: Zhongnan Daxue Xuebao, 46, 1715–1722, doi: 10.11817/j.issn.1672-7207.2015.05.020.

Zhang, L., J. Li, Z. Li, J. Zhang, R. Zhu, and Y. Bao, 2014, Advances in shale oil/gas research in North America and considerations on exploration for continental shale oil/gas in China: Advances in Earth Science, 29, 700–711.

Zhou, Q., N. Song, C. Wang, B. Li, X. Wang, C. Peng, and Y. Ren, 2014, Geological evaluation and exploration prospect of Huayuan shale gas block in Hunan Province: Natural Gas Geoscience, 25, 130–140, doi: 10.11764/j.issn.1672-1926.2014.01.0130.

Figures

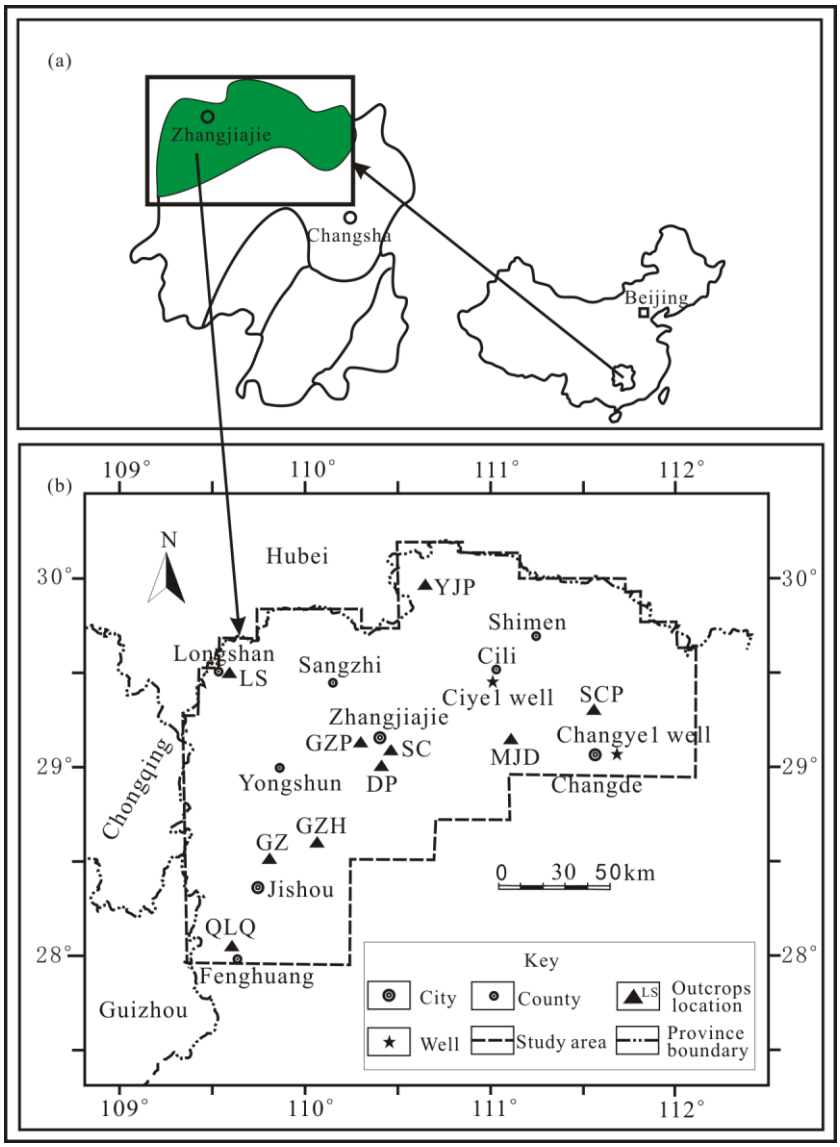

Fig. 1. (a) Outline map of China showing position of Hunan province and study area (in green). (b) Enlargement of the study area from Fig. 1a showing sampling locations.

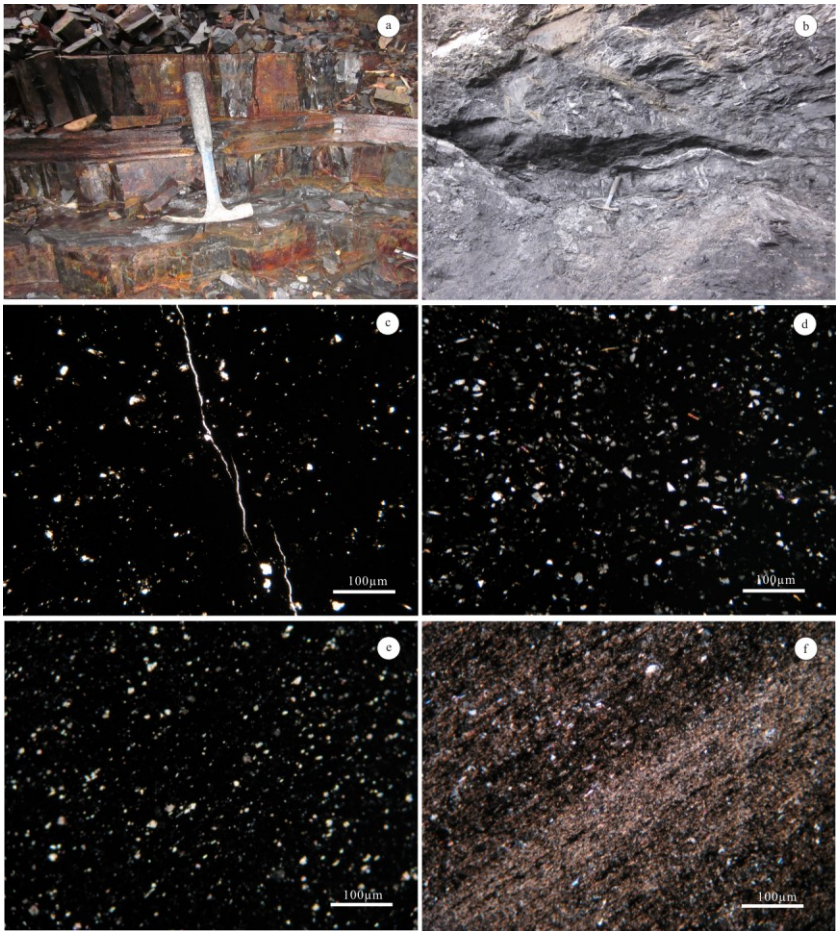

Fig. 2. Outcrop and micro-photographic images of the lower Cambrian aged Niutitang Shale. (a) Siliceous shale with well-developed tension joints, Guzhe outcrop; (b) Shale with well-developed shear joints, Ganziping outcrop; (c) Siliceous shale (sample GZH01) - the dark is mainly organic matter and the light is mainly quartz, and fractures are currently sealed by quartz; (d) Non-laminated shale (sample GZH04) in which microphotograph exhibits an homogeneous matrix, and organic matter (dark; TOC=8.34%) occupies significant area in the texture and scatters in the matrix; (e) Non-laminated shale (SC06): organic matter aggregates or particles are distributed without orientation in the matrix, and the TOC content is relatively high (TOC=8.58%); (f) Laminated shale (YJP03): well developed laminae are shown by the orientation of quartz (41.9%), clay mineral (49.9%) and organic matter (dark), and the TOC content is relatively low (TOC=1.56%).

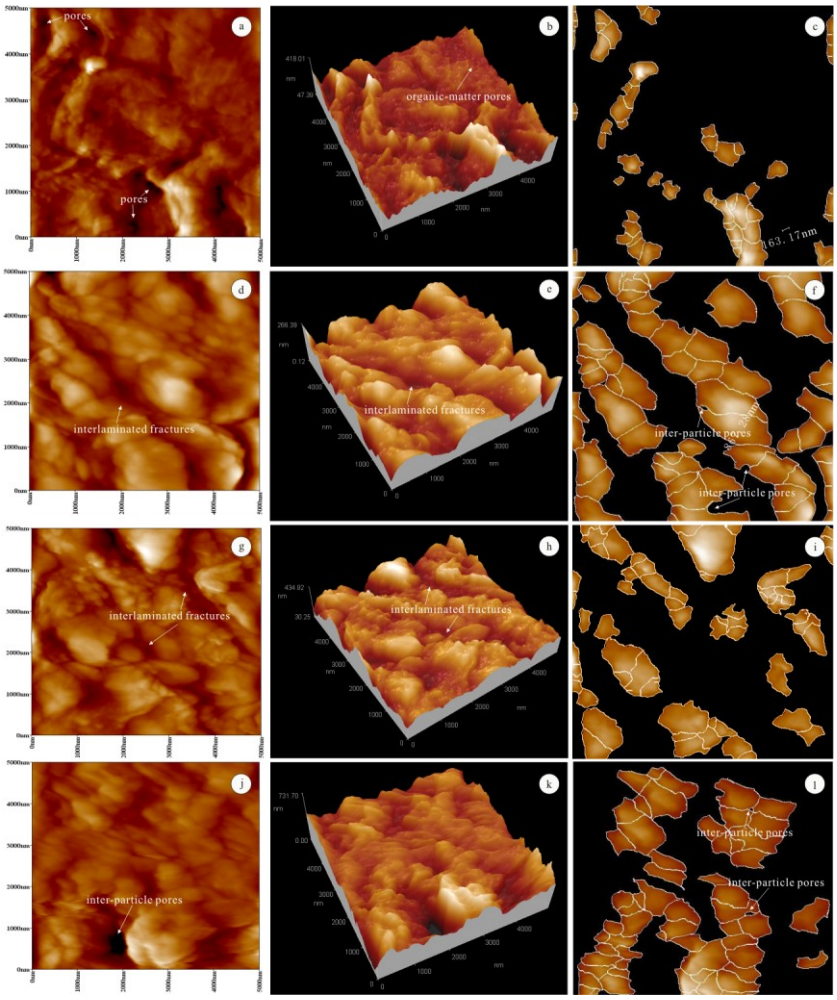

Fig. 3. Scanning Probe Microscopy topographical images of surfaces of selected Niutitang Shale samples. (a)–(c) The two-dimensional and three-dimensional topographical images, and mineral distribution image of the carbonaceous shale sample (sample YJP02; TOC=13.46) surface with the size of 5×5mm, respectively: void space (e.g., pores and fractures) and organic matter are characterized by the black colour, while mineral particles correspond to the bright colour in the panel c; Mineral particles and organic matter are distributed without orientation, and "honeycomb" organic-matter pores are well developed; (d)-(f) The two-dimensional and three-dimensional topographical images, and mineral distribution image of the silty shale sample (sample QLQ04; TOC=0.77) surface with the size of 5×5mm: laminae are shown by the orientation of minerals and organic matter, and inter-

particle pores and fractures with good connectivity are relatively well developed; (g)-(i) The two-dimensional and three-dimensional topographical images, and mineral distribution image of the siliceous shale sample (sample MJD01; TOC=2.62) surface with the size of 5×5mm: laminae are shown by the orientation of minerals and organic matter, and fractures with good connectivity are relatively well developed; (j)-(l) The two-dimensional and three-dimensional topographical images, and mineral distribution image of the black shale sample (sample GZ01; TOC=9.39) surface with the size of 5×5mm: mineral particles and organic matter are distributed without orientation, and inter-particle pores are relatively well developed.

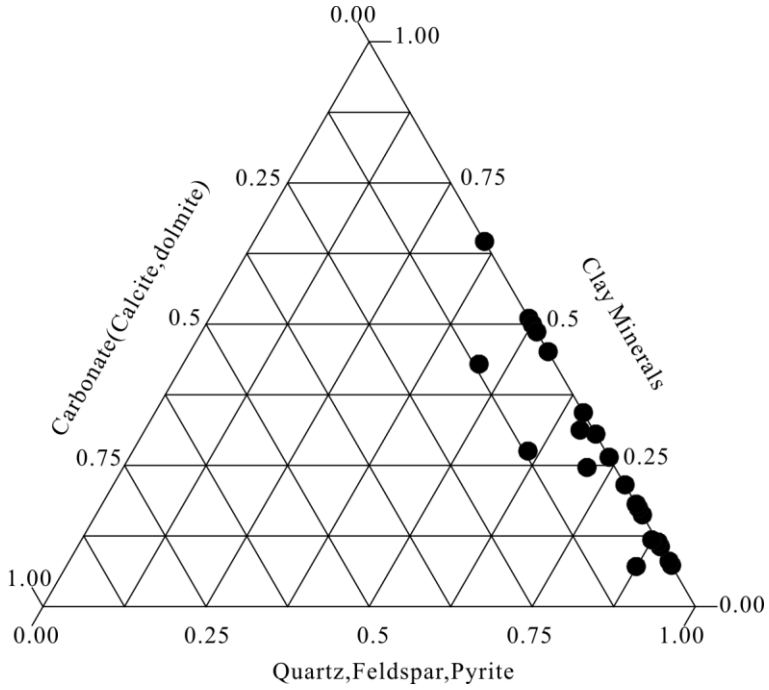

Fig. 4. Ternary diagram of mineral constituents.

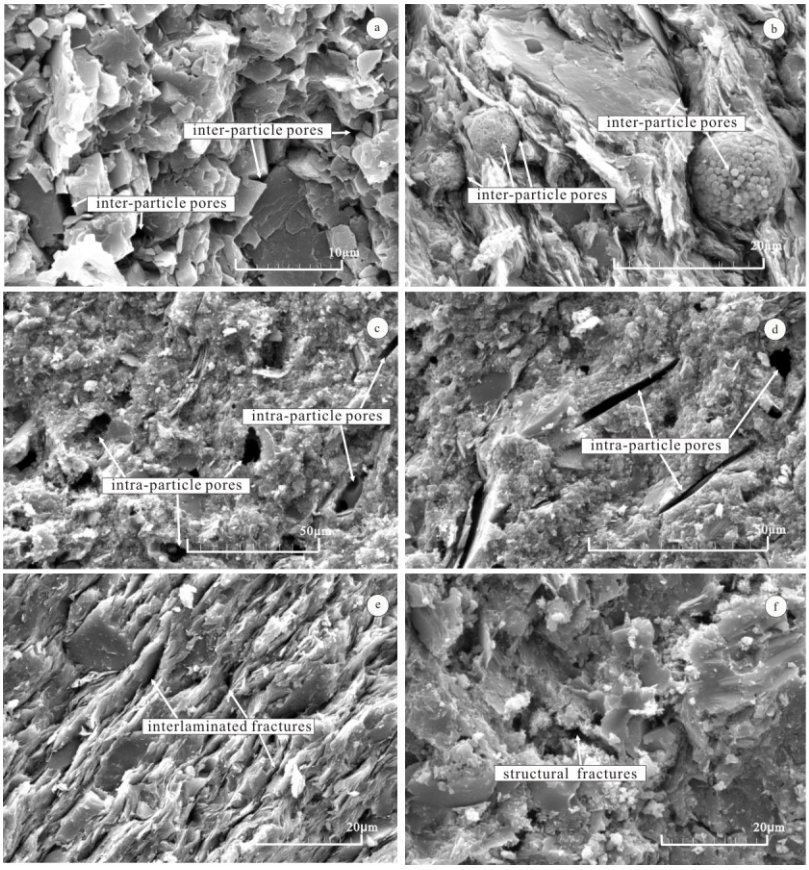

Fig. 5. Scanning Electron Microscope images of shales from the Niutitang Formation showing in (a) and (b) inter-particle pores, in (c) and (d) intra-particle pores, in (e) interlaminated fractures, and in (f) structural fractures.

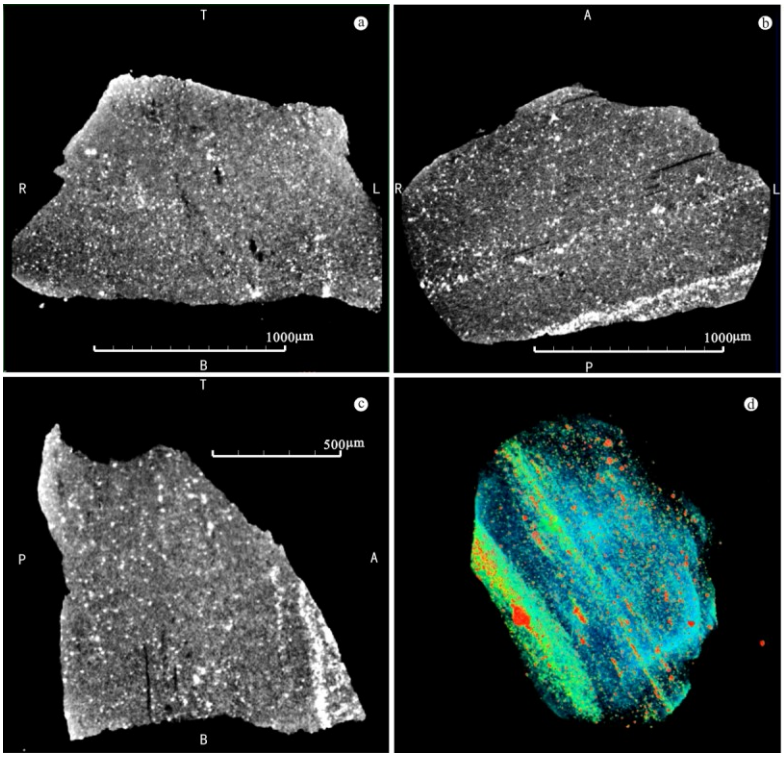

Fig. 6. CAD 3D-view of pores (black spot), fractures (black line), minerals (white area), and shale organic matrix (gray area) of the sample (sample SC03): (a) an image on the x–z plane, showing the posterior (P)-anterior (A) direction; (b) an image on the x–y plane, showing the top (T)-bottom (B) direction; (c) an image on the y–z plane, showing the right (R)-left (L); (d) the 3D-view image shows the distribution of fractures. The lines in this figure represent fractures.

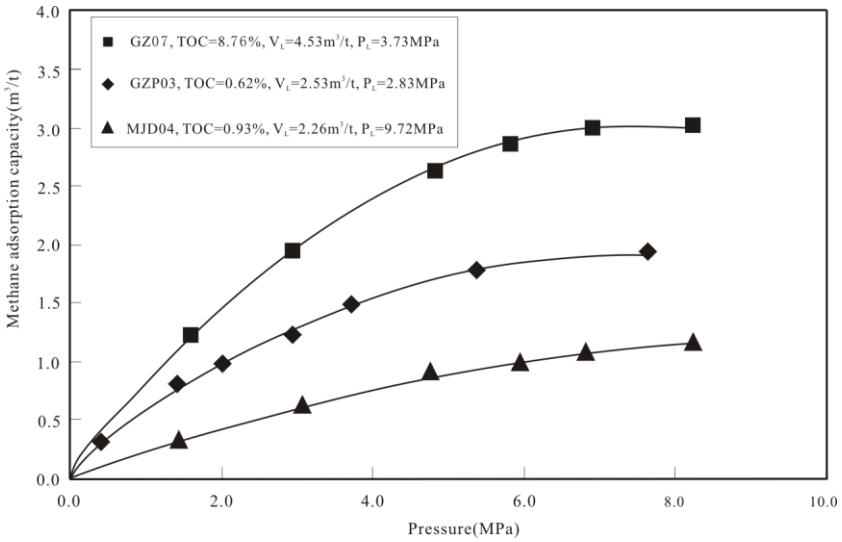

Fig. 7. Methane adsorption isotherms (at 40 °C) for Niutitang Shale samples.

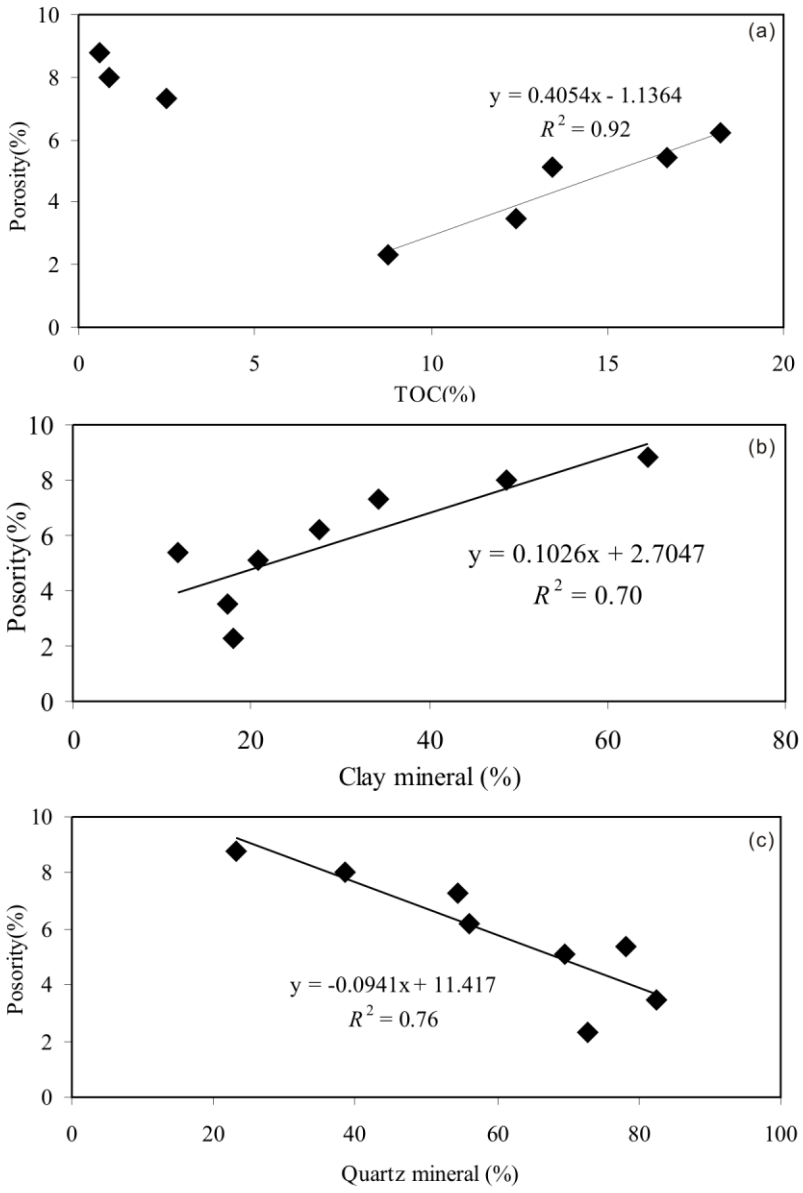

Fig. 8. Correlation plots of porosity with (a) TOC content, (b) clay mineral content, and (c) quartz content for the Niutitang Shale in the northwest Hunan.

Tables

Table 1. Total Organic Carbon (TOC) and bitumen reflectance (Rb) values for the Lower Cambrian Niutitang Shale in northwest Hunan.

Sections (code)	TOC (%)			equal-Ro (%)		
	Min value	Max value	Mean value	Min value	Max value	Mean value
Longshan(LS)	1.6	3.6	2.6	2.5	2.9	2.7
Qiliangqiao(QLQ)	0.8	6.8	3.5	3.1	3.1	3.1
Guzhe(GZ)	1.8	12.4	3.8	2.6	3.8	3.2
Guzhang(GZH)	1.8	14.9	3.8	3.0	3.8	3.5
Ganziping(GZP)	0.6	10.8	7.5	3.1	3.7	3.5
Shancha(SC)	0.9	13.4	7.8	3.3	4.3	3.7
Daping(DP)	1.0	9.2	6.3	3.2	3.5	3.3
Yangjiaping(YJP)	1.6	13.5	3.5	3.0	3.6	3.4
Majindong(MJD)	0.9	12.2	6.3	2.8	3.4	3.0
Shichaipo(SCP)	2.2	18.2	7.2	2.5	2.8	2.7

Table 2. Values of Total Organic Carbon (TOC), equivalent vitrinite reflectance (equal-Ro) and X-ray diffraction (XRD) Mineralogy for representative shale samples from the Lower Cambrian Niutitang Shale in northwest Hunan.

ID	samples	Lithofacies	TOC (%)	equal-Ro (%)	feldspar (%)	quartz (%)	carbonate (%)	dolomite (%)	pyrite (%)	gypsum (%)	clay (%)	others (%)
1	GZP03	dark-grey shale	0.6	3.5	9.9	23.2	0.0	0.0	2.3	0.0	64.6	0.0
2	GZP05	black shale	4.4	3.7	3.7	80.1	0.0	0.0	0.0	0.0	16.2	0.0
3	GZP06	black shale	8.2	3.7	1.6	60.0	0.9	3.4	9.5	0.0	24.6	0.0
4	SC01	dark-grey shale	0.9	3.4	11.8	38.5	0.0	0.0	1.1	0.0	48.6	0.0
5	SC03	black shale	7.2	4.3	3.5	53.2	0.0	0.0	5.5	10.5	27.3	0.0
6	SC06	black shale	8.6	3.3	1.5	43.8	0.0	11.9	15.3	0.0	27.5	0.0
7	GZ01	black shale	9.4	2.6	8.7	64.9	0.0	0.0	0.0	0.0	26.4	0.0
8	GZ03	black carbonaceous shale	12.4	3.8	0.0	82.6	0.0	0.0	0.0	0.0	17.4	0.0
9	GZ07	black shale	8.8	3.3	9.0	72.9	0.0	0.0	0.0	0.0	18.1	0.0
10	GZH01	black siliceous shale	2.6	3.0	2.7	86.5	0.0	0.0	0.0	0.0	7.0	3.8
11	GZH03	black carbonaceous shale	14.9	3.8	5.0	80.9	0.0	0.0	3.1	0.0	11.0	0.0
12	GZH04	black shale	8.3	3.6	15.3	65.4	0.0	0.0	0.0	0.0	18.0	1.3
13	DP01	argillaceous dolomite	1.6	3.2	0.4	16.7	2.3	78.7	0.0	0.0	1.9	0.0
14	DP04	black shale	6.3	3.5	3.5	78.3	3.1	2.9	5.4	0.0	6.8	0.0
15	DP05	dark-grey siliceous shale	1.0	3.2	1.2	87.4	0.0	0.0	0.0	0.0	11.4	0.0
16	QLQ02	dark-grey shale	1.4	3.0	11.1	31.0	1.5	10.2	3.3	0.0	42.9	0.0
17	QLQ04	dark-grey silty mudstone	0.8	3.1	10.2	37.0	0.0	0.0	1.8	0.0	51.0	0.0
18	YJP02	black carbonaceous shale	13.5	3.5	6.6	69.6	0.0	0.0	0.0	0.0	20.9	2.9
19	YJP03	dark-grey shale	1.6	3.6	5.6	41.9	0.0	0.0	2.6	0.0	49.9	0.0
20	YJP05	black siliceous shale	2.2	3.0	3.5	88.5	0.0	0.0	0.0	0.0	8.0	0.0
21	MJD01	black siliceous shale	2.6	3.0	2.1	87.4	0.0	0.0	0.0	0.0	10.5	0.0
22	MJD04	dark-grey shale	0.9	2.8	9.2	38.2	0.0	0.0	7.5	0.0	45.1	0.0
23	MJD06	black carbonaceous shale	12.2	3.0	3.8	70.5	0.0	0.0	0.0	0.0	25.7	0.0
24	MJD08	black shale	2.5	3.4	11.2	54.5	0.0	0.0	0.0	0.0	34.3	0.0
25	SCP02	black carbonaceous shale	18.2	2.5	0.0	56.0	0.0	1.8	3.0	0.0	27.6	11.6
26	SCP05	black carbonaceous shale	16.7	2.8	9.3	78.2	0.0	0.8	0.0	0.0	11.7	0.0

Table 3. Rock Density, Porosity, and Permeability for the Lower Cambrian aged Niutitang Shale in the northwest Hunan.

ID	samples	TOC (%)	Rock density (g/cm^3)	porosity (%)	Permeability (mD)
1	GZP03	0.6	2.42	8.8	0.0600
4	SC01	0.9	2.46	8.0	0.0500
8	GZ03	12.4	2.13	3.5	0.0018
9	GZ07	8.8	2.20	2.3	0.0096
18	YJP02	13.5	2.00	5.1	0.0085
24	MJD08	2.5	2.35	7.3	0.0225
25	SCP02	18.2	1.98	6.2	0.0098
26	SCP05	16.7	2.04	5.4	0.0082